Reduction in Radiation Noise Level for Inductive Power Transfer Systems using Spread Spectrum Techniques

Kent Inoue, *Student Member, IEEE*, Keisuke Kusaka, *Member, IEEE*, and Jun-ichi Itoh, *Senior Member, IEEE*

***Abstract*-- Two proposed methods of reducing radiation noise caused by inductive power transfer (IPT) systems using spread spectrum techniques were experimentally demonstrated. In IPT systems for electric vehicles (EVs) or plug-in hybrid EVs (PHEVs), noise reduction techniques are necessary because the radiation noise from the IPT system for EVs or PHEVs must not exceed the limits defined by noise standards, such as the well-known regulation set by the International Special Committee on Radio Interference (CISPR). In the proposed methods, the radiation noise from the transmission coils of the IPT system is spread in the frequency domain by randomly changing the output frequency of the inverter. The output frequency is selected according to the generation of pseudorandom numbers. In the first proposed method, spread spectrum with a uniform distribution (SSUD), the output frequency is selected from the frequency range of 80 to 90 kHz with an even distribution. In the second method, spread spectrum with a biased distribution (SSBD), the output current of the inverter is considered. The possibility of selecting an output frequency in the given range is biased in proportion to the combined impedance from the transmission coil and the resonance capacitors on the primary side. In experiments with a 3-kW prototype, when SSUD and SSBD were applied, the fundamental components of the radiation noise were suppressed by 4.45 and 8.27 dBμA, respectively, in comparison with the noise obtained using the conventional system, which operates the inverter at a fixed frequency.**

***Index Terms*—Inductive power transfer, Wireless power transfer, Spread spectrum, Radiation noise, Electromagnetic interference.**

I. Introduction

In recent years, inductive power transfer (IPT) systems have been actively studied and developed [1–7]. In particular, the practical realization of IPT systems for electric vehicles (EVs) or plug-in hybrid EVs (PHEVs) is highly desired because IPT systems are capable of improving the usability of EVs and PHEVs [8–12]. IPT systems transmit power using the weak magnetic coupling between a primary coil and a secondary coil through a large air-gap [13]. The fundamental principle IPT systems are the same as that of a transformer. However, coupling coefficient between the primary and secondary coils is typically in the range of k = 0.1 to 0.3, in IPT systems. In modern IPT systems, compensation circuits, which contain capacitors and inductors, are used to compensate for the power factor from the perspective of the power supply [1] [8] [10]. Compensation circuits reduce the copper loss that occurs in the windings of coils and the power loss in power supply.

To use IPT systems in a practical applications, radiated electromagnetic noise must be suppressed [14] to satisfy exiting standards, such as the well-known standard based on CISPR11, a standard by the International Special Committee on Radio Interference, because the IPT system must not affect other wireless communication systems, or electronic equipment.

A common noise reduction method is the use of a filter circuit. In this method, a low-pass filter is connected to the input stage of the primary coil. The filter circuit suppresses the harmonic components of the current that flow into the transmission coil. However, the power loss of the filter is large in this method because the cut-off frequency of the filter circuit must be close to the fundamental frequency. As previous studies, suppression methods using a magnetic or metal shield have been proposed [15–18]. The transmission coils are surrounded by plates composed of a magnetic material or metal. The radiation noise can be suppressed because these shields alter the magnetic flux to produce eddy currents. However, the eddy currents increase the power loss of the IPT system. Additionally, the presence of an aperture for the magnetic path must be ensured in the IPT system. Thus, the shielding can only provide partial suppression of the radiation noise. Previous studies [19] [20] have proposed a noise reduction method involving the formation of the current that flows in the coils by using a primary converter. However, additional switches are required to reduce the radiation noise. Previous study [21] has proposed a reduction method that involves the use of a set of two inverters and two coils in close alignment. In this setup, the radiation noise is cancelled by passing opposite-phase currents through the two coils. However, the inclusion of two inverters and two coils increases the cost of the IPT system.

Alternatively, spread spectrum techniques are widely used in motor drive systems with a pulse width modulation (PWM) inverter [22–24]. This technique is called random carrier PWM. The carrier frequency of the PWM inverter is continuously changed during operation to reduce acoustic noise. By changing the carrier frequency, the frequency

Manuscript received December 20, 2016; revised April 4, 2017; accepted May 18, 2017.

Kent Inoue, Keisuke Kusaka and Jun-ichi Itoh are with the Dept. Electrical Electronics and Information, Nagaoka University of Technology, Niigata 940-2188, Japan (e-mail: k_inoue@stn.nagaokaut.ac.jp; kusaka@vos.nagaokaut.ac.jp; itoh@vos.nagaokaut.ac.jp).

components of the acoustic noise caused by winding vibrations can be spread over wide range in the frequency domain [22–24]. Spread spectrum techniques are also used in converters to reduce conducted electromagnetic interference (EMI) [25–27]. In both applications, the carrier frequency is changed to suppress acoustic or electromagnetic noise. However, spread spectrum techniques have not been applied to square wave inverters, meaning that they have not been applied to IPT systems.

In this paper, two methods of reducing the radiation noise for the IPT system based on the spread spectrum technique are proposed and demonstrated with the experimental results. In the first proposed method, spread spectrum with a uniform distribution (SSUD), the radiation noise is suppressed by selecting the output frequency from a uniform probability distribution. In the second proposed method, spread spectrum with a biased distribution (SSBD), the output frequency is selected from a biased probability distribution. The probability distribution is proportional to the impedance combined from compensation capacitor and the transmission coil on the primary side.

This paper is organized as follows. In section II, the electromagnetic noise regulations for the IPT system are described. The two proposed noise reduction methods are explained in section III. Section IV describes the implementation of the proposed methods in a 3-kW prototype. The radiation noise of the IPT system using the proposed methods is then evaluated. Finally, the effects of the spread spectrum technique on the system efficiency are assessed.

II. Allowable Radiation Noise Level

Fig. 1 shows the radiation noise regulations for IPT systems with an output power of 7-kW or less [28]. The regulations are currently under discussion for standardization. The use of a frequency range from 79 to 90 kHz is considered for IPT systems of EVs. This regulation basically corresponds to CISPR11 Group 2, Class B [29]. However, the radiation noise from the frequency range of 79 to 90 kHz must be mitigated to a maximum of 68.4 dBμA/m. Moreover, the maximum radiation noise in higher frequency bands (150–490 kHz) will be mitigated by 10 dBμA from CISPR Class B.

Furthermore, in the IPT system, a limit to the allowable radiation noise in the range 9 to 150 kHz must be imposed. The radiation noise in all frequency bands except that from 79 to 90 kHz must be lower than 23.1 dBμA/m. Similarly, the allowable limit in the frequency band from 526.5 to 1606.5 kHz is −2.0 dBμA/m because this frequency band has been used for amplitude modulation (AM) broadcasting.

It should be note that CISPR11 suggest measuring the noise using a quasi-peak measurement method. As stated in the regulations, not only the fundamental frequency component of the radiation noise but also its harmonic components should be suppressed.

III. Noise Reduction Methods By Spread Spectrum

A. Compensation Circuits.

Fig. 2 shows the typical circuit configuration of the IPT system with a series–series (S/S) compensation [30]. In the IPT system for EVs, the primary coils are buried in roads or parking lots, and secondary coils are installed the bottoms of the cars. For this reason, the magnetic coupling between the primary and secondary coils are weak. A large leakage inductance attributable to this weak magnetic coupling causes the reactive power to increase. To solve these problems, compensation circuits, such as series–series (S/S) compensation, or series–parallel (S/P) compensation circuits, are widely used to compensate the leakage inductance [31].

When an input voltage V_1 is applied to the primary side, the primary and secondary currents are calculated as

$$\dot{I}_1 = \frac{r_2 + R_{eq} + j\left(\omega L_2 - \frac{1}{\omega C_2}\right)}{\left\{r_1 + j\left(\omega L_1 - \frac{1}{\omega C_1}\right)\right\}\left\{r_2 + R_{eq} + j\left(\omega L_2 - \frac{1}{\omega C_2}\right)\right\} + \omega^2 L_m^2}\dot{V}_1 \quad (1)$$

$$\dot{I}_2 = \frac{j\omega L_m}{\left\{r_1 + j\left(\omega L_1 - \frac{1}{\omega C_1}\right)\right\}\left\{r_2 + R_{eq} + j\left(\omega L_2 - \frac{1}{\omega C_2}\right)\right\} + \omega^2 L_m^2}\dot{V}_1 . \quad (2)$$

where R_{eq} is the equivalent load considering the rectifier; r_1 and r_2 are the equivalent series resistances of the primary and secondary windings, respectively; L_1 and L_2 are the primary

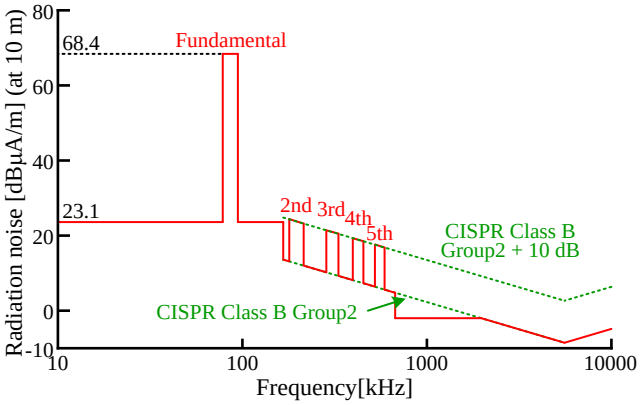

Fundamental	79 kHz – 90 kHz
2nd	158 kHz – 180 kHz
3rd	237 kHz – 270 kHz
4th	316 kHz – 360 kHz
5th	395 kHz – 450 kHz

Fig. 1 Maximum allowable radiation noise for IPT systems of 7-kW or less for use in EVs (under discussion).

and secondary inductances, respectively; C_1 and C_2 are the primary and secondary compensation capacitors, respectively; L_m is the mutual inductance; and ω is the angular frequency of the power supply. Note that the voltage V_1 is the fundamental component of the output voltage of the inverter. The equivalent load is given by [31]

$$R_{eq} = \frac{8}{\pi^2}\frac{V_{2,DC}^2}{P_2}. \quad (3)$$

where $V_{2,DC}$ is the secondary direct current (DC) voltage and P_2 is the output power.

The compensation capacitors are generally selected to cancel out the reactive power at the input frequency. Thus, the compensation capacitors can be calculated

$$C_1 = \frac{1}{L_1\omega^2}, \quad (4)$$

$$C_2 = \frac{1}{L_2\omega^2}. \quad (5)$$

The primary current with the compensation is given by

$$\dot{I}_1 = \frac{r_2 + R_{eq}}{r_1(r_2 + R_{eq}) + \omega^2 L_m^2}\dot{V}_1. \quad (6)$$

Because of presence of the compensation circuit, the input impedance from the perspective of the output of the power supply is relatively low. Thus, the input current contains a large fundamental component.

The radiation noise is mainly caused by the current flowing through the primary and secondary coils. For other converters, shielding with a magnetic material or metal is an effective method of suppressing radiation noise. However, in an IPT system, the presence of an aperture for the magnetic path must be ensured to supply the power. Thus, shielding provides a limited solution for the suppression of radiation noise.

B. Proposed Noise Reduction Methods.

In the methods proposed in this paper, the radiation noise is spread in the frequency domain by changing the output frequency of the voltage source inverter in two different ways. The output frequency is selected at random in range of 80 to 90 kHz. In SSUD, the output frequency of the voltage source inverter is selected from a discrete uniform probability distribution. In contrast, SSBD involves selecting the output frequency of the voltage source inverter from a biased probability distribution. The probability distribution is biased to be proportional to the combined impedance of the transmission coil and the compensation capacitor on the primary side. Because of this biased probability distribution, the harmonic components of the current output from the inverter are spread.

Fig. 3 shows the probability distributions of the output frequency of the inverter. Fig. 3 (a) is the probability distribution of SSUD [32]. The probability distribution is a discrete uniform distribution from 80 to 90 kHz. This means that each output frequency has the same probability of being selected. The frequency parameter is discrete because the carrier for the modulation of the inverter is generated in a free-programmable gate array (FPGA). The output frequency is renewed at every carrier. Selecting the output frequency of the voltage source inverter from a uniform distribution causes the harmonic components of the voltage to be evenly spread. Fig. 3 (b) shows the probability distribution of SSBD [33]. The input impedance of the IPT system depends on the frequency. Thus, the probability distribution is proportional to the impedance from the transmission coil and combined with that from the compensation capacitor. Fig. 4 shows the harmonic components of the primary current around the fundamental frequency range (80–90 kHz). In the SSUD, the current in the coils is not taken into the consideration because the output frequency of the voltage source inverter is selected from the uniform distribution. Thus, the current in the coils has a frequency characteristic depending on the impedance of the IPT system. On the other hand, considering the impedance of

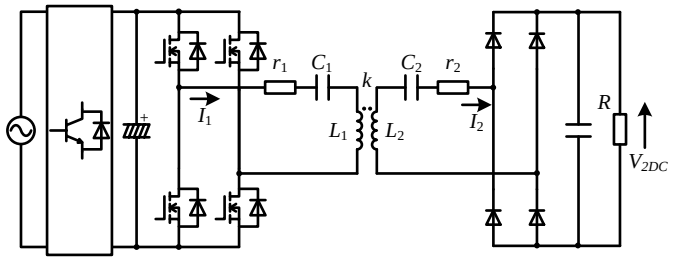

Fig. 3 Typical system configuration of IPT systems for EVs.

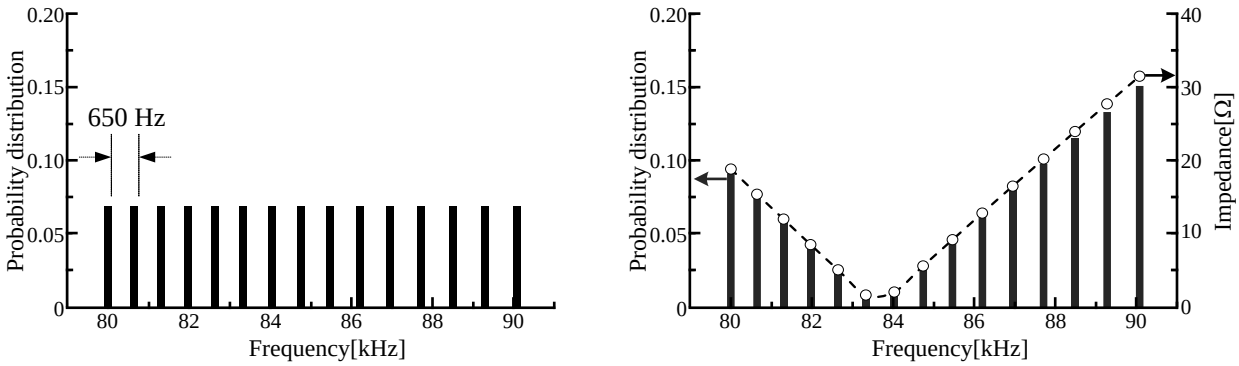

Fig. 2 Probability distributions for the proposed spread spectrum techniques. (a) Proposed method I: SSUD. (b) Proposed method II: SSBD.

the IPT system, the SSBD selects the output frequency from the biased distribution. It helps further spreading the current harmonics around the fundamental frequency in the frequency domain in comparison with constant frequency operation and the SSUD. Thus selecting the output frequency of the voltage source inverter from the biased distribution is effective to reduce the noise. Note that the probability distribution, which is proposed in the paper, is not actually an optimum distribution because the probability distribution was introduced through a trial and error process.

Table I shows the assignment of the pseudorandom numbers for the output frequency using SSUD (Table I (a)) and SSBD (Table I (b)). The output frequency is selected according to the generation of 7-bit pseudorandom numbers.

Fig. 5 shows the pseudorandom number generation method. The pseudorandom numbers are generated using a maximal length sequence (M-sequence) [25] [34] in the digital signal processor (DSP). Different pseudorandom number generation methods can be used. However the generation method using an M-sequence was selected for use in this study because a complex generation method for pseudorandom numbers is not suitable as an algorithm for DSP-based implementation. An M-sequence random number is generated as the exclusive OR of $X_{Z\text{-}p}$ and $X_{Z\text{-}q}$ as shown

$$X_Z = X_{Z-p} \oplus X_{Z-q}, \tag{7}$$

where $X_{Z\text{-}p}$ and $X_{Z\text{-}q}$ are the present values of X_Z delayed by periods of p and q, respectively, with $p > q$. In this study, $p = 7$ and $q = 1$ were used. Moreover, the pseudorandom number is a 7-bit number.

IV. Experimental Results

A. Experimental Setup.

Fig. 6 and Table II show the configuration for the prototype and the specifications, respectively. In these experiments, a 420-V DC voltage power supply was used. SiC MOSFETs and SiC diodes were used at switching devices. The SiC MOSFETs are controlled by the FPGA and the DSP.

The inductances of the primary and secondary coils were designed according to the following equation [11] assuming the effect of the spread spectrum can be ignored;

$$L_1 = \frac{R_{eq}}{\omega_0 k_0} \frac{V_{1,DC}^2}{V_{2,DC}^2}, \tag{8}$$

$$L_2 = \frac{R_{eq}}{\omega_0 k_0}. \tag{9}$$

where ω_0 is the center frequency of the frequency range used for the spread spectrum. The compensation circuit can be calculated from the center frequency ω_0 using (4) and (5). This means that the compensation circuits are designed to resonate at 85.1 kHz.

Fig. 7 shows the primary and secondary coils for the prototype. Solenoid-type coils [35] are used as the transmission coils. The transmission distance is 150 mm, assuming transmission from the road to the bottom of the EV or PHEV.

B. Radiation Noise Measurement Conditions.

Fig. 8 shows the setup of the probe (ELECTRO-METRICS EM-6993) used to measure the radiation noise. The radiation noise was measured at two points, A and B, and the distance from the edge of the transmission coils and to each measurement position was 500 mm. Both measurement points are in the center of the transmission coils along the *z*-axis. At position A, the flux, crossing the *x*-*y* and *y*-*z* planes were measured. At position B, the flux crossing the *y*-*z* plane was measured.

The measurements were conducted in a shielded room. These measurements cannot satisfy the requirements for the measurement of radiated emissions established by CISPR in terms of the measurement environment. The standards require measurements to be conducted with a 10-m test range anechoic chamber, which eliminates unwanted noise at a frequency of 85 kHz with good performance. Thus, in this paper, only the results of the radiation noise reduction obtained using a conventional system and the currently proposed methods are compared.

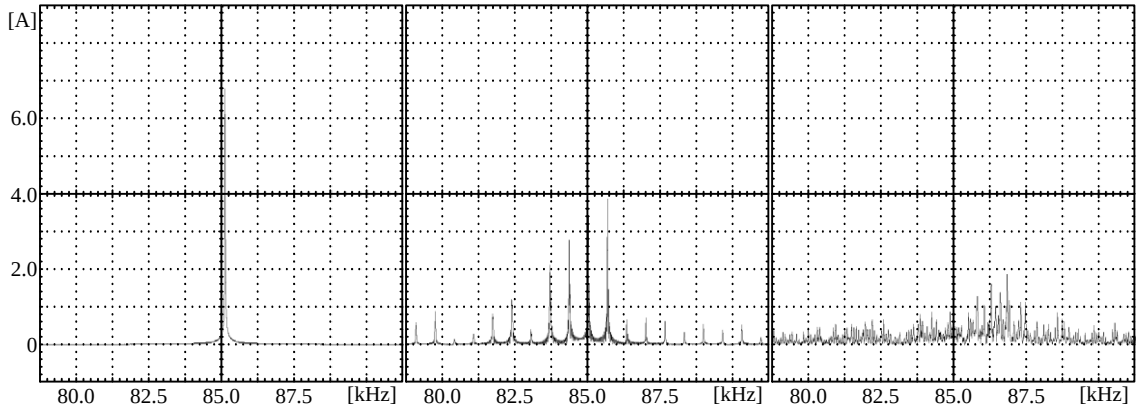

Fig. 4 Probability distributions for the proposed spread spectrum techniques. (a) Constant frequency. (b) Proposed method I: SSUD. (c) Proposed method II: SSBD.

TABLE I ASSIGNMENT OF THE OUTPUT FREQUENCY. (A) PROPOSED METHOD I: SSUD. (B) PROPOSED METHOD II: SSBD.

	pseudorandom number	Frequency [kHz]		pseudorandom number	Frequency [kHz]
1	0000001	80.00	65	1000001	85.47
⋮	⋮	80.00	⋮	⋮	85.47
8	0001000	80.00	72	1001000	85.47
9	0001001	80.65	73	1001001	86.21
⋮	⋮	80.65	⋮	⋮	86.21
16	0010000	80.65	80	1010000	86.21
17	0010001	81.30	81	1010001	86.96
⋮	⋮	81.30	⋮	⋮	86.96
24	0011000	81.30	88	1011000	86.96
25	0011001	81.97	89	1011001	87.72
⋮	⋮	81.97	⋮	⋮	87.72
32	0100000	81.97	96	1100000	87.72
33	0100001	82.64	97	1100001	88.50
⋮	⋮	82.64	⋮	⋮	88.50
40	0101000	82.64	104	1101000	88.50
41	0101001	83.33	105	1101001	89.29
⋮	⋮	83.33	⋮	⋮	89.29
48	0110000	83.33	112	1110000	89.29
49	0110001	84.03	113	1110001	90.09
⋮	⋮	84.03	⋮	⋮	90.09
56	0111000	84.03	120	1111000	90.09
57	0111001	84.75			
⋮	⋮	84.75			
64	1000000	84.75			

	pseudorandom number	Frequency [kHz]		pseudorandom number	Frequency [kHz]
1	0000001	80.00	42	0101010	85.47
⋮	⋮	80.00	⋮	⋮	85.47
11	0001011	80.00	47	0101111	85.47
12	0001100	80.65	48	0110000	86.21
⋮	⋮	80.65	⋮	⋮	86.21
20	0010100	80.65	55	0110111	86.21
21	0010101	81.30	56	0111000	86.96
⋮	⋮	81.30	⋮	⋮	86.96
27	0011011	81.30	65	1000001	86.96
28	0011100	81.97	66	1000010	87.72
⋮	⋮	81.97	⋮	⋮	87.72
32	0100000	81.97	77	1001101	87.72
33	0100001	82.64	78	1001110	88.50
⋮	⋮	82.64	⋮	⋮	88.50
35	0100011	82.64	91	1011011	88.50
36	0100100	83.33	92	1011100	89.29
37	0100101	84.03	⋮	⋮	89.29
38	0100110	84.75	108	1101100	89.29
⋮	⋮	84.75	109	1101101	90.09
41	0101001	84.75	⋮	⋮	90.09
			127	1111111	90.09

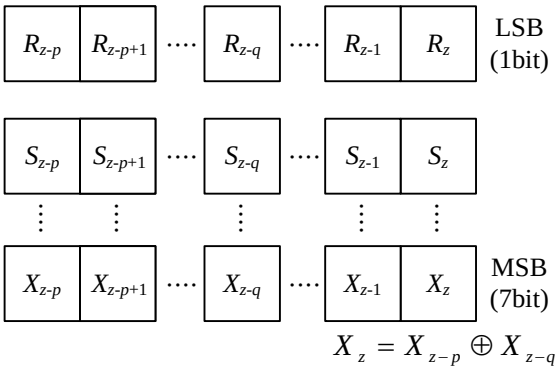

Fig. 5 Generation method of 7-bit pseudorandom numbers based on a maximal length sequence.

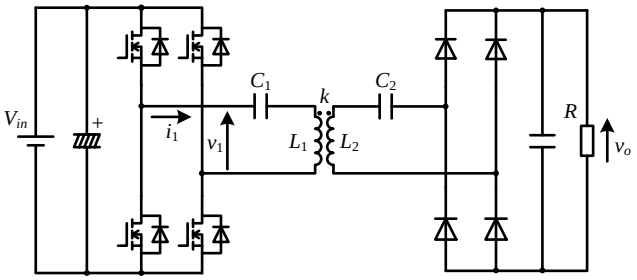

Fig. 6 Experimental setup.

TABLE II SPECIFICATIONS OF PROTOTYPE.

	Symbol	Value
Input DC voltage	V_{in}	420 V
Coupling coefficient	k	0.20
Primary inductance	L_1	392 μH
Secondary inductance	L_2	401 μH
Primary capacitance	C_1	8.96 nF
Secondary capacitance	C_2	8.78 nF
Transmission distance	l	150 mm
MOSFETs	SCH2080KEC (ROHM)	
Diodes	SCS220AE (ROHM)	
Ferrite plates	PC40 (TDK)	

C. Operation Waveforms.

Fig. 9 shows the operation waveforms. In all operation methods, the output power is fixed at 3.0 kW. Fig. 9 (a) shows the waveforms obtained using the conventional method with

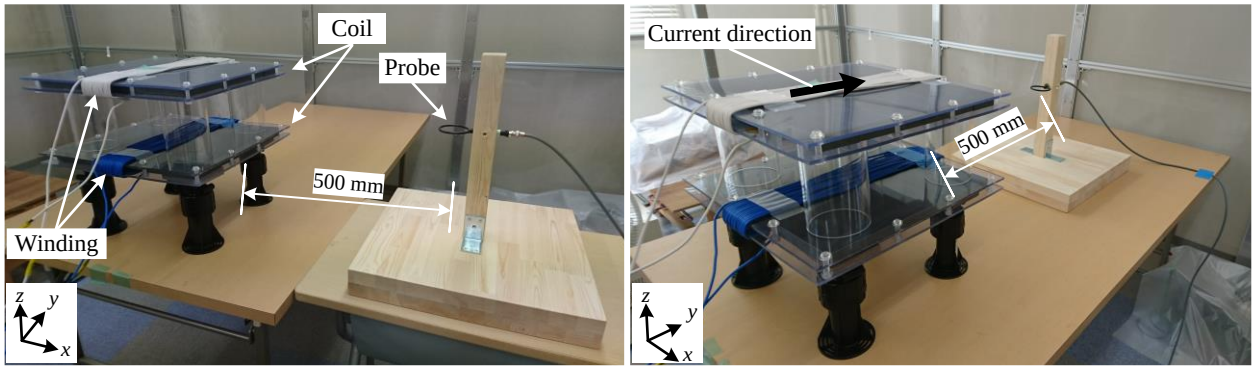

Fig. 8 Radiation noise measurement setup.

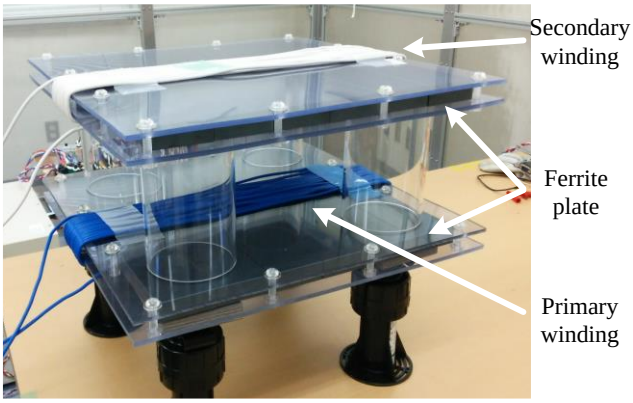

Fig. 7 Transmission coils with a rated power of 3-kW (Solenoid-type coils).

the output frequency fixed at 85.1 kHz. Fig. 9 (b) and (c) show the waveforms obtained using SSUD and SSBD, respectively. The output frequency of the voltage source inverter in these cases is selected randomly according to Table I (a) and (b), respectively. To obtain the results shown in Fig. 9 (b) and (c), the output frequency was varied from 80 to 90 kHz at fixed time intervals according to the generated pseudorandom numbers. When the proposed methods are used, the amplitude of the primary current i_1 varies. However, constant output voltages were obtained for all operation methods.

D. Radiation Noise.

Figs. 10–11 show the radiation noise at point A in the *x*-*y* and *y*-*z* planes defined in Fig. 8. Fig. 12 shows the radiation noise at point B in the *y*-*z* plane defined in Fig. 8. In Figs. 10–12, subpart (a) shows the results obtained using the conventional method, and subparts (b) and (c) show the results obtained using SSUD and SSBD, respectively. When the conventional method was used, the fundamental and low-order harmonic components sharply appeared. When the proposed methods were used, the maximum value for the fundamental and low-order harmonics were suppressed. When SSUD and SSBD were used, the harmonic components around the fundamental frequency were suppressed by 4.45 and 8.27 dBμA in comparison with the conventional method, which operates the inverter at a fixed frequency. In the same manner, the low-order harmonic components were suppressed in comparison with the conventional method. Both of the proposed methods can be used to suppress these components.

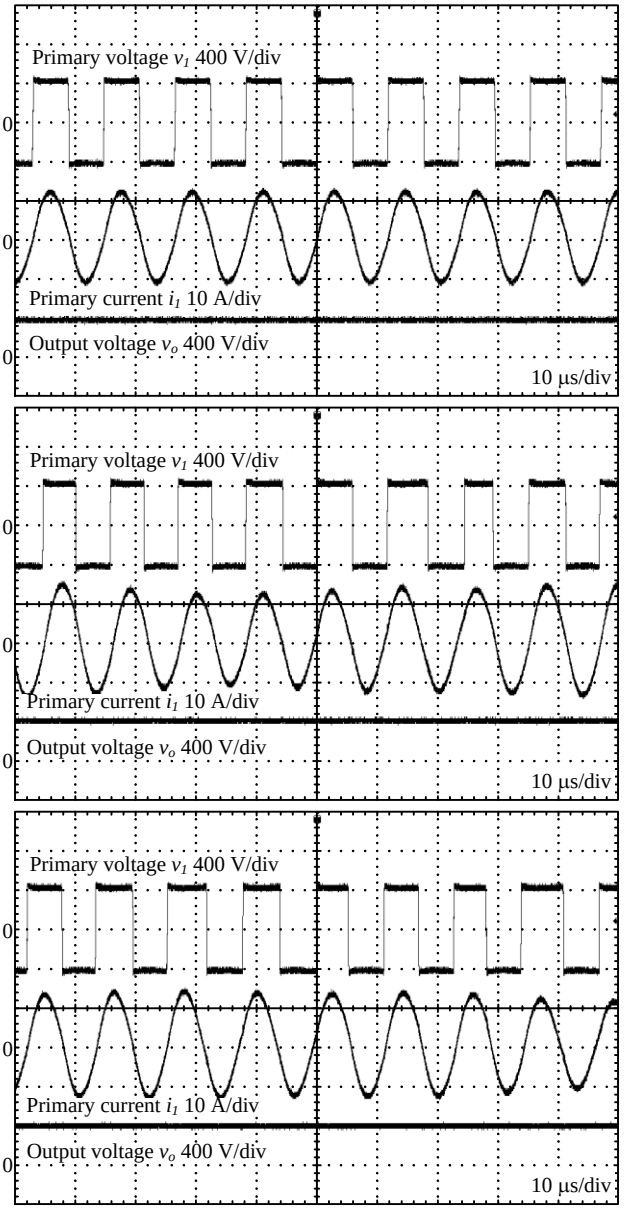

Fig. 9 Operation waveforms of the IPT system. (a) Constant frequency. (b) Proposed method I: SSUD. (c) Proposed method II: SSBD.

However, in the operation with SSUD, the harmonic components peaked at 85.1 kHz. This was caused by the frequency dependence of the impedance. In addition, the proposed method causes higher noise floor due to the change

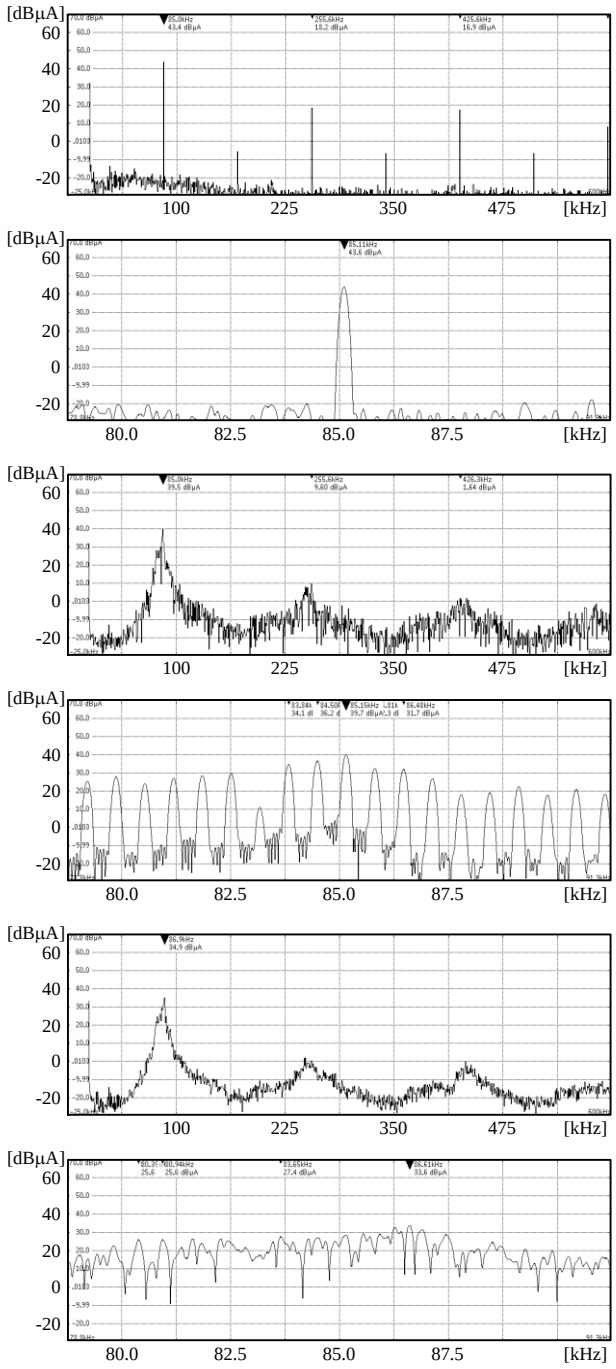

Fig. 10 Radiation noise (Point A, *x*-*y* plane). (a) Constant frequency. (b) Proposed method I: SSUD. (c) Proposed method II: SSBD.

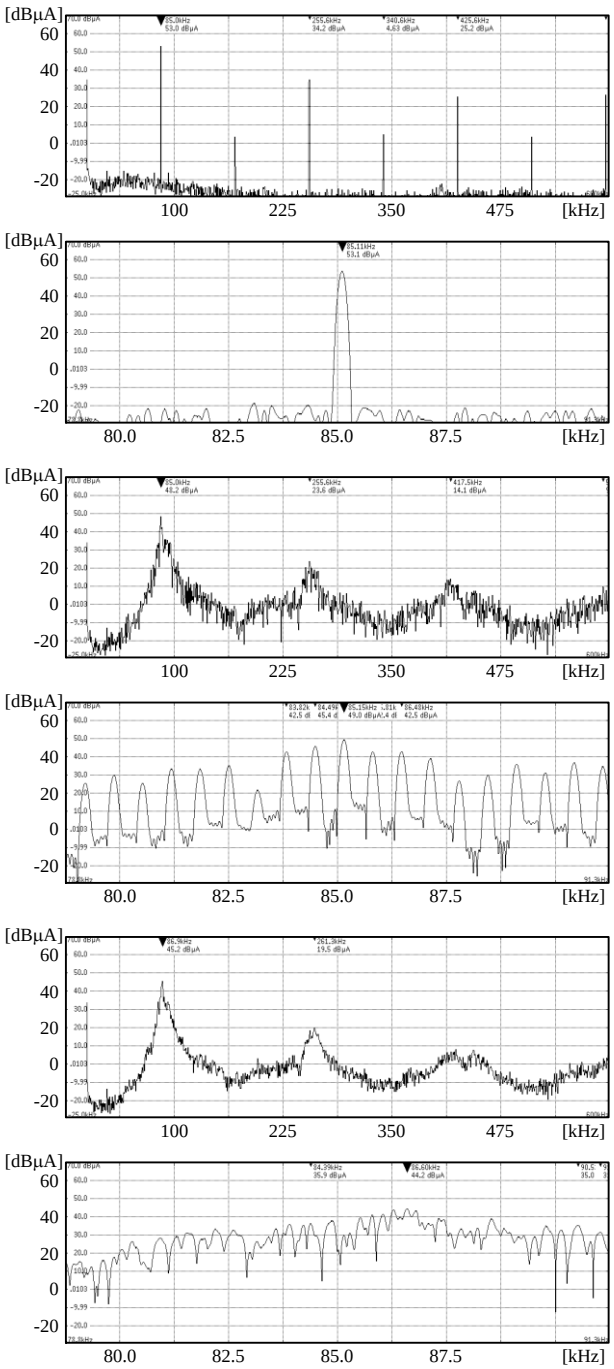

Fig. 11 Radiation noise (Point A, *y*-*z* plane). (a) Constant frequency. (b) Proposed method I: SSUD. (c) Proposed method II: SSBD.

of the output frequency. The proposed system should be evaluated whether it satisfies the regulation. However, the measurement method for the regulation (e. g. measurement environment, equipment) are still in discussion. It is expected that the proposed system will be evaluated after the official regulation is established.

E. Efficiency Evaluation.

Fig. 13 shows the DC-to-DC efficiency characteristics for the conventional and two proposed methods. The efficiency is defined as the ratio of the input DC power to the output DC power. All of the curves show similar characteristics. The maximum efficiency was 94.9% at an output power of 3.0 kW when the inverter was operated at a fixed frequency. In contrast, the maximum efficiency was 94.1% at an output power of 3.0 kW when SSUD was used. The decrease in the efficiency is caused by the increased reactive current due to the difference between the operating and resonance frequencies. The reactive current increases the copper loss, iron loss, conduction loss, and switching loss on the converter. Hence, the decrease in efficiency with the SSUD was 0.8% at the rated load. When SSBD was used, the maximum efficiency was 93.8% at the rated load. The decrease in the efficiency was 1.1% in comparison with that of the

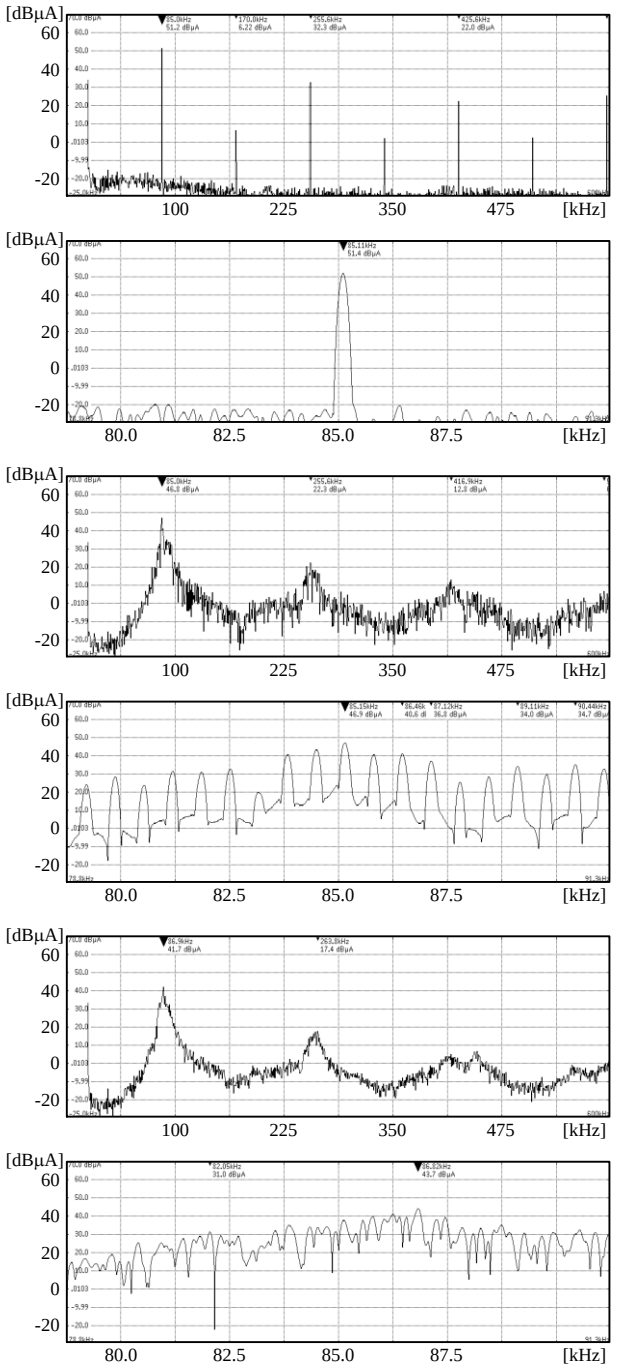

Fig. 12 Radiation noise (Point B, *y*-*z* plane). (a) Constant frequency. (b) Proposed method I: SSUD. (c) Proposed method II: SSBD.

conventional method. Thus, using SSBD is effective in the heavy-load region. In contrast, the efficiency drops by a maximum of 4.4% when the output power is 1.0 kW. In the light-load region, the effect of the no-load loss is larger than that in the heavy-load region. However, the current in the windings is smaller than that in the heavy-load region. Considering that the radiation noise is proportional to the current, weak suppression of the radiation noise can be acceptable in the light-load region. Therefore, in the light-load region, SSUD should be used.

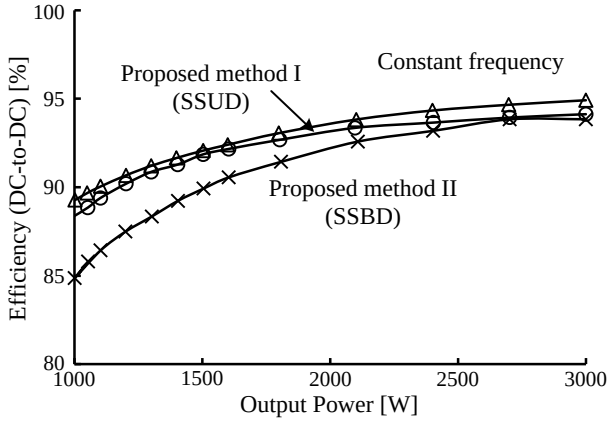

Fig. 13 Efficiency characteristics.

V. Conclusion

In this paper, two methods for the reduction of the radiation noise of an inductive power transfer system were proposed and experimentally demonstrated. The radiation noise from the transmission coils for the IPT system was spread in the frequency domain by changing the output frequency of the voltage source inverter at random. This eliminates the necessary of additional components, such as a noise shield and a filter circuit, in the proposed methods. In the first proposed method, called SSUD, the output frequency of the voltage source inverter is selected from the range of 80 to 90 kHz from a discrete uniform probability distribution. In the second proposed method, called SSBD, the output frequency is selected from a biased discrete probability distribution. The probability distribution is proportional to the combined impedance from the transmission coil and the compensation capacitor on the primary side considering the frequency characteristics of the IPT system. Because of this bias, the frequency components of the output current, which flows through the transmission coils, was from 80 to 90 kHz. From the experimental results with the 3.0 kW prototype, the harmonic components around the fundamental frequency of radiation noise were suppressed by 4.45 and 8.27 dBμA by applying SSUD and SSBD, respectively. Therefore, SSBD was more effective than SSUD and the conventional method in the suppression of the noise expect in the heavy-load region. In the light-load region, using SSBD can be greatly decrease the DC-to-DC efficiency because of the no-load loss, which dominates the loss. Thus, SSUD is a more suitable reduction method in the light-load region because SSUD provides radiation noise reduction with a small decrease in the efficiency in comparison with the conventional method.

References

[1] S. Y. R. Hui, W. Zhong, C. K. Lee: "A Critical Review of Recent Progress in Mid-Range Wireless Power Transfer," *IEEE Trans. Power Electron.*, vol. 29, no. 9, pp. 4500-4511, Sep. 2014.

[2] D. Shimode, T. Mura, S. Fujiwara, "A Study of Structure of Inductive Power Transfer Coil for Railway Vehicles," *IEEJ J. Ind. Appl.*, vol. 4, no. 5, pp. 550-558, Sep. 2015

[3] Y. Hayashi, Y. Chiku, "Contactless DC Connector Concept for High-Power –Density 380-V DC Distribution System," *IEEJ J. Ind. Appl.*, vol. 4, no. 1, pp. 49-58, Jan. 2015.
[4] K. Kusaka, K.Orikawa, J. Itoh, I. Hasegawa, K. Morita, T. Kondo, "Galvanic Isolation System with Wireless Power Transfer for Multiple Gate Driver Supplies of a Medium-voltage Inverter," *IEEJ J. Ind. Appl.*, vol. 5, no. 3, pp. 206-214, May. 2016.
[5] T. Mizuno, T. Ueda, S. Yashi, R. Ohtomo, Y. Goto, "Dependence of Efficiency on Wire Type and Number of strands of Litz Wire for Wireless Power Transfer of Magnetic Resonant Coupling," *IEEJ J. Ind. Appl.*, vol. 3, no. 1, pp. 35-40, Jan. 2014.
[6] N. K. Trung, T. Ogata, S. Tanaka, K. Akatsu, "Analysis and PCB Design of Class D Inverter for Wireless Power Transfer Systems Operating a 13.5 MHz," *IEEJ J. Ind. Appl.*, vol. 4, no. 6, pp. 703-713, Nov. 2015.
[7] J. T. Boys, G. A. Covic, Y. Xu: "DC Analysis Technique for Inductive Power Transfer Pick-Ups," *IEEE Trans. Power Electron.*, vol. 1, no. 2, pp. 51-53, Jun. 2003.
[8] Siqi Li, Chunting C. Mi: "Wireless Power Transfer for Electric Vehicle Applications," *IEEE J.*, vol.3, no.1, pp.4-17, Apr. 2015.
[9] T. Shijo, K. Ogawa, S. Obayashi: "Optimization of Thickness and Shape of Core Block in Resonator for 7 kW-Class Wireless Power Transfer," *IEEE Energy Conversion Congr. Expo*, pp. 3099-3012, Sep. 2015.
[10] R. Ota, N. Hoshi, J. Haruna, "Design of Compensation Capacitor in S/P Topology of Inductive Power Transfer System with Buck or Boost Converter on Secondary Side," *IEEJ J. Ind. Appl.*, vol. 4. no. 4, pp. 476-485, Jul. 2015
[11] R. Bosshard, J. W. Kolar, J. Muhlethaler, I. Stevanovic, B. Wunsch, F. Canales: "Modeling and η-α-Pareto Optimization of Inductive Power Transfer Coils for Electric Vehicles," *IEEE J.*, vol. 3, no. 1, pp. 50-64, Mar. 2014.
[12] R. Haldi, K. Schenk: "A 3.5 kW Wireless Charger for Electric Vehicles with Ultra High Efficiency," *IEEE Energy Conversion Congr. Expo*, pp. 668-674, Sep. 2014.
[13] T. Imura, Y. Hori: "Maximizing Air Gap and Efficiency of Magnetic Resonant Coupling for Wireless Power Transfer Using equivalent Circuit and Neumann Formula," *IEEE Trans. Ind. Electron.*, vol. 58, no. 10, pp. 4746-4752, Feb. 2011.
[14] J. Kim, H. Kim, M. Kim, S. Ahn, J. Kim, J. Kim: "Analysis of EMF Noise from the Receiving Coil Topologies for Wireless Power Transfer," *Asia-Pacific Symp. Electromagnetic Compatibility*, pp. 645-648, May 2012.
[15] M. Jo, Y. Sato, Y. Kaneko, S. Abe: "Methods for Reducing Leakage Electric Field of a Wireless Power Transfer System for Electric Vehicles," *IEEE Energy Conversion Congr. Expo*, pp. 1762-1769, Sep. 2014.
[16] H. Kim, J. Cho, S. Ahn, J. Kim, J. Kim: "Suppression of Leakage Magnetic Field from a Wireless Power Transfer System using Ferrimagnetic Material and Metallic Shielding," *IEEE Int. Symp. Electromagnetic Compatibility*, pp. 640-645, Aug. 2012.
[17] T. Campi, S. Cruciani, M. Feliziani: "Magnetic Shielding of Wireless Power Transfer Systems," *IEEE Int. Symp. Electromagnetic Compatibility*, pp. 422-425, May 2014.
[18] K. Maikawa, K. Imai, Y. Minagawa, M. Arimitsu, H. Iwao: "Magnetic Field Reduction Technology of Wireless Charging System," *JSAE Congr. Autumn*, no. 110-13, Oct. 2013.
[19] K. Kusaka, J. Itoh: "A Suppression Method of Radiated Emission caused by Low-order Harmonic Current in a Wireless Power transfer System," *IEEJ Annu. Meeting*, no. 4-117, pp. 196-197, Mar. 2015.
[20] D. Narita, T. Imura, H. Fujimoto, Y. Hori: "Electromagnetic Field Suppression in Polyphase Wireless Power Transfer via Magnetic Resonance Coupling," *Tech. rep. of IEICE*, pp.39-44, Jun. 2014.
[21] T. Shijo, K. Ogawa, M. Suzuki, Y. Kanekiyo, M. Ishida, S. Obayashi: "MI Reduction Technology in 85 kHz Band 44 kW Wireless Power Transfer System for Rapid Contactless Charging of Electric Bus," *IEEE Energy Conversion Congr. Expo*, Sep. 2016.
[22] A. M. Trzynadlowski, F. Blaabjerg, J. K. Pedersen, R. L. Kirlin, S. Legowski, "Random Pulse Width Modulation Techniques for Converter-Fed Drive Systems – A Review," *IEEE Trans. Ind. Appl.*, vol. 30, no. 5, pp. 1166-1175, Sep. 1994.
[23] J. T. Boys, P. G. Handley, "Spread spectrum switching: low noise modulation technique for PWM inverter drives," *IEE Proc. B – Elect. Power Appl.*, vol. 139, no. 3, pp. 252-260, May 1992.
[24] C. M. Liaw, Y. M. Lin, C. H. Wu, K. I. Hwu, "Analysis, Design, and Implementation of a Random Frequency PWM Inverter," *IEEE Trans. Power Electron.*, vol. 15, no. 5, pp. 843-854, Sep. 2000.
[25] K. Kim, Y. Jung, Y. Lim, "A New Hybrid Random PWM Scheme," *IEEE Trans. Power Electron.*, vol. 24, no. 1. pp. 192- 200, Feb. 2009.
[26] K. K. Tse, H. S. Chung, S. Y. Hui, H. C. So, "Analysis and Spectral Characteristics of a Spread-Spectrum Technique for Conducted EMI Suppression," *IEEE Trans. Power Electron.*, vol. 15, no. 2. pp. 399-410, Mar. 2000.
[27] D. Stone, B. Chambers, D. Howe, "Random Carrier Frequency Modulation of PWM Waveforms to Ease *Electromagnetic Compatibility* Problems in Switched Mode Power Supplies," *Int. Conf. on Power Electron. Drive Syst.*, pp. 16-21, Feb. 1995.
[28] Ministry of Internal Affairs and Communications, Japan, "Inquiry of technical requirements for wireless power transfer system for EVs in technical requirements for wireless power transfer system in standards of International Special Committee on Radio Interference (CISPR)," 2015.
[29] CISPR 11: 2015, "Industrial, scientific and medical equipment – Radio-frequency disturbance characteristics – Limits and methods of measurement," 2015.
[30] Y. H. Sohn, B. H. Choi, E. S. Lee, G. C. Lim, G. Cho, C. T. Rim: "General Unified Analyses of Two-Capacitor Inductive Power Transfer Systems: Equivalence of Current-Source SS and SP Compensations," *IEEE Trans. Power Electron.*, vol. 30, no. 11, pp. 6030-6045, Mar. 2015.
[31] R. L. Steigerwald, "A Comparison of Half-Bridge Resonant Converter Topologies," *IEEE Trans. Power Electron.* vol. 3, no. 2, pp. 174-182, Apr. 1988.
[32] K. Kusaka, K. Inoue, J. Itoh: "Reduction in Radiation Noise Level for Inductive Power Transfer System with Spread Spectrum", *The Int. Elect. Vehicle Technol. and Automotive Power Electron. Japan Conf.*, May 2016.
[33] K. Inoue, K. Kusaka, J. Itoh: "Reduction on Radiation Noise Level for Inductive Power Transfer Systems with Spread Spectrum focusing on Combined Impedance of Coils and Capacitor," *IEEE Energy Conversion Congr. Expo*, Sep. 2016.
[34] F. J. MacWilliams, N. J. A. Sloane, "Pseudo-random sequences and arrays," *Proc. of the IEEE*, vol. 64, no. 12, pp. 1715-1729, Dec. 1976.
[35] G. A. Covic, J. T. Boys, "Modern Trends in Inductive Power Transfer for Transportation Application," *IEEE J.*, vol. 1, no. 1. pp. 29-41, May 2013.

Kent Inoue (S'16) was born in Ibaraki, Japan, in 1993. He received his B.S. degrees in electrical, electronics and information engineering from Nagaoka University of Technology, Niigata, Japan in 2016. He has been with Nagaoka University of Technology as a M.S. course student in electrical, electronics and information engineering. His current research interests includes an inductive power transfer system.

Mr. Inoue is a student member of the Institute of Electrical Engineers of Japan and the IEEE.

Keisuke Kusaka (S'13, M'16) was born in Miyagi, Japan, in 1989. He received his B.S. and M.S. degrees in electrical, electronics and information engineering from Nagaoka University of Technology, Niigata, Japan in 2011, 2013, respectively. From 2015 to 2016, he was with Swiss Federal Institute of Technology in Lausanne (EPFL), Switzerland as a trainee. In 2016, he received his Ph.D. degree in energy and environment science from Nagaoka University of Technology. Since 2016, he has been with Nagaoka University of Technology, Niigata, Japan as a researcher. His current research interests include the areas of inductive power transfer systems and high-frequency converters.

Dr. Kusaka is a member of the Institute of Electrical Engineers of Japan, the Society of Automotive Engineers of Japan and the IEEE.

Jun-ichi Itoh (M'04, SM'13) was born in Tokyo, Japan, in 1972. He received his M.S. and Ph.D. degree in electrical and electronic systems engineering from Nagaoka University of Technology, Niigata, Japan in 1996, 2000, respectively. From 1996 to 2004, he was with Fuji Electric Corporate Research and Development Ltd., Tokyo, Japan. He was with Nagaoka University of Technology, Niigata, Japan as an associate professor. Since 2017, he has been a professor. His research interests are matrix converters, dc/dc converters, power factor correction techniques, energy storage system and adjustable speed drive systems.

He received IEEJ Academic Promotion Award (IEEJ Technical Development Award) in 2007. In addition, he also received Isao Takahashi Power Electronics Award in IPEC-Sapporo 2010 from IEEJ, 58th OHM Technology Award from The Foundation for Electrical Science and Engineering, November, 2011, Intelligent Cosmos Award from Intelligent Cosmos Foundation for the Promotion of Science, May, 2012, and Third prize award from Energy Conversion Congress and Exposition-Asia, June, 2013. Prizes for Science and Technology (Development Category) from the Commendation for Science and Technology by the Minister of Education, Culture, Sports, Science and Technology, April 2017.

Dr. Itoh is a senior member of the Institute of Electrical Engineers of Japan, the Society of Automotive Engineers of Japan and the IEEE.